

Experimental investigation of the thermal transport properties of a carbon nanohybrid dispersed nanofluid†

Tessy Theres Baby and Sundara Ramaprabhu*

Received 28th December 2010, Accepted 28th February 2011

DOI: 10.1039/c0nr01024c

A hybrid nanostructure consisting of 1D carbon nanotubes and 2D graphene was successfully synthesized. Nanofluids were made by dispersing the hybrid nanostructure in deionized (DI) water and ethylene glycol (EG) separately, without any surfactant. Later the thermal conductivity and heat transfer coefficient of the nanofluids were experimentally measured. Meanwhile, multiwalled carbon nanotubes (MWNT) were prepared by catalytic chemical vapor deposition (CCVD), and hydrogen exfoliated graphene (HEG) was synthesized by exfoliating graphite oxide in a hydrogen atmosphere. The hybrid nanostructure (f-MWNT+f-HEG) of functionalized MWNT (f-MWNT) and functionalized HEG (f-HEG) was prepared by a post mixing technique, and the sample was characterized by powder X-ray diffraction, Raman spectroscopy, field emission scanning electron microscopy and transmission electron microscopy. Thermal conductivity of the nanofluids was measured for different volume fractions of f-MWNT+f-HEG at different temperatures. The hybrid nanostructure dispersed in the DI water based nanofluid shows a thermal conductivity enhancement of 20% for a volume fraction of 0.05%. Similarly, for a Reynolds number of 15 500, the enhancement of the heat transfer coefficient is about 289% for a 0.01% volume fraction of f-MWNT+f-HEG.

1. Introduction

Owing to their unique properties, like high surface area, high mechanical strength and high thermal and electrical conductivity, 2D graphene and 1D multiwalled carbon nanotubes (MWNT) find applications in sensors,^{1,2} storage,^{3,4} and energy.⁵ Synthesizing high quality material in large quantities is one of the limitations for commercializing the use of these materials. Novoselov *et al.*⁶ first prepared graphene by micro-mechanical cleavage. Even though one can get single layer graphene, the quantity of graphene obtained by this method is very low. Graphene has also been synthesized by other techniques like vacuum exfoliation,⁷ thermal exfoliation,⁸ chemical exfoliation,⁹ chemical vapor deposition,¹⁰ hydrogen exfoliation¹¹ *etc.* Similarly, there are different techniques for the synthesis of MWNT like chemical vapor deposition (CVD), laser ablation, and arc melting.^{12–14}

Recently, researchers have succeeded in making a new hybrid nanostructure which is a mixture of MWNT and graphene. This hybrid nanostructure has been used in supercapacitors,¹⁵ transparent conductors,¹⁶ and as an electrode material for lithium ion batteries.¹⁷ One of the main advantages of hybrid materials is that they combine the merits of their constituents, thereby

performing better than any of the individual constituents. A Monte Carlo computational model reveals the existence of a novel 3D carbon material, consisting of parallel graphene layers stabilized by vertically aligned carbon nanotubes (CNT) in between the graphene planes. In the case of the MWNT and graphene hybrid material, MWNT help to avoid stacking of graphene sheets, thereby increasing the surface area.¹⁵

Nanomaterials dispersed in base fluids are called nanofluids. Choi, Eastman and co-workers^{18,19} coined the term nanofluid. The conventional fluids like deionized (DI) water and ethylene glycol (EG) have low thermal conductivity compared to solid materials. In order to improve the efficiency of a cooling system, one has to use highly thermally conductive fluids. MWNT and graphene have high thermal conductivity in their solid form.^{20–22} There are reports on the enhancement of thermal properties by the use of nanomaterials in conventional base fluids.^{18,23,24} Recently, Yu *et al.* have shown an enhancement in thermal conductivity of a nanofluid containing graphite oxide.²⁵ In our previous work we have shown an enhancement in the thermal conductivity of thermally exfoliated graphene dispersed DI water and EG based nanofluids.²⁶ Another important factor which affects the efficiency of a nanofluid is the convective heat transfer coefficient. Ding *et al.*²⁷ reported an enhancement in the heat transfer coefficient of 350% for nanofluids containing 0.5 wt.% carbon nanotubes. Park *et al.*²⁸ highlighted that a graphene/graphitic oxide nanosheet (GON) dispersed water based nanofluid can be exploited to maximize the critical heat flux (CHF) most efficiently by building up a characteristically ordered

Alternative Energy and Nanotechnology Laboratory (AENL), Nano Functional Materials Technology centre (NFMTc), Department of Physics, Indian Institute of Technology, Madras, India. E-mail: ramp@iitm.ac.in; Fax: +91-44-22570509; Tel: +91-44-22574862

† Electronic supplementary information (ESI) available: Analysis of Raman data. See DOI: 10.1039/c0nr01024c

porous surface structure, which occurs due to its self-assembling characteristic that results in a geometrically changed critical instability wavelength.

In the present work, a hybrid nanostructure (f-MWNT+f-HEG) was synthesized by a post-mixing technique. Further, the hybrid nanostructure was used for synthesizing nanofluids by dispersing it in DI water and EG. The thermal conductivity and heat transfer properties of these nanofluids were measured. The graphene used in the present study was synthesized by the hydrogen exfoliation technique by which large quantities of graphene can be synthesized. The MWNT were synthesized by catalytic chemical vapor deposition (CCVD). Before mixing, the MWNT and HEG were functionalized separately by acid treatment. The thermal conductivity and heat transfer measurement of nanofluids were done for different volume fractions of f-MWNT+f-HEG in DI water and EG as base fluids. Heat transfer studies were carried out using an home-made setup.

2. Experimental

2.1. Materials and methods

Graphite (99.99%, 45 μm) was purchased from Bay Carbon, Inc USA. All other reagents, sulfuric acid, nitric acid, potassium permanganate (KMnO_4), sodium nitrate, ethylene glycol and hydrogen peroxide (H_2O_2), were analytical grade. DI water was used throughout the experiment.

Synthesis of MWNT has been described elsewhere.²⁹ In short, they were synthesized using CCVD using an alloy hydride catalyst. Acetylene gas was used as the carbon precursor and was allowed to pass through the furnace at around 700 $^\circ\text{C}$. An inert atmosphere was maintained inside the furnace throughout the experiment to avoid oxidation of the catalyst and also as a carrier gas for the hydrogen and acetylene. Several purification procedures were adopted in order to purify the as grown MWNT. After purification by oxidation in air and acid treatment, the MWNT were washed with deionized water until the pH became neutral. The sample was then filtered and dried at 80 $^\circ\text{C}$.

Graphite oxide (GO) was prepared from graphite using the Hummers method.³⁰ Briefly, 2 g of graphite was treated with 46 ml of sulfuric acid in an ice bath. 1 g of sodium nitrate was added slowly to the above solution, followed by the addition of 6 gm of potassium permanganate. The mixture was left at room temperature for some time and a specific quantity of water was added to the mixture. After 15 min, the suspension was treated with hydrogen peroxide. The mixture was filtered and the filter cake was washed with a copious quantity of DI water. Lastly, the suspension was again filtered and dried in a vacuum oven at 40 $^\circ\text{C}$ for 8 h. Graphene was synthesized by exfoliating dried graphite oxide in a hydrogen atmosphere.¹¹ In short, GO was kept in a tubular furnace which was flushed with Ar for 15 min. At around 200 $^\circ\text{C}$ hydrogen was allowed in for a period of 1 min. The resulting hydrogen exfoliated graphene was named HEG.

The as-synthesized HEG was not soluble in water because during exfoliation the oxygen containing functional groups were removed from the sample making it hydrophobic. In order to make it hydrophilic, HEG was functionalized with concentrated H_2SO_4 : HNO_3 in the ratio 3 : 1. The acid treatment was done by ultrasonicing the sample in the acid medium for 3 h, and the

mixture was further washed several times with DI water, filtered and dried in a vacuum. The same procedure was adopted for functionalizing the MWNT. The hybrid nanostructure was prepared by mixing equal amounts of f-MWNT and f-HEG in a specified volume of water after functionalization. Further, the solution was ultrasonicated for 1 h and stirred for 24 h. The final mixture was filtered, dried and used for making nanofluids.

The samples were characterized with various techniques. Powder X-ray diffraction (XRD) studies were carried out using a PANalytical X'PERT Pro X-ray diffractometer with nickel-filtered Cu $K\alpha$ radiation as the X-ray source. The pattern was recorded in the 2θ range of 5 $^\circ$ to 90 $^\circ$ with a step size of 0.016 $^\circ$. The Raman spectra were obtained with a WITEC alpha 300 Confocal Raman spectrometer equipped with an Nd:YAG laser (532 nm) as the excitation source. Field emission scanning electron microscopy (FESEM) and transmission electron microscopy (TEM) images were taken using FESEM, FEI QUANTA and JEOL TEM-2010F instruments, respectively. The nanofluid was prepared by dispersing a known amount of nanohybrid in the base fluid with the help of an ultrasonicator. Ultrasonication was done for a period of 30–45 min. The thermal conductivity of the nanofluids was measured using a KD2 Pro thermal property analyzer (Decagon, Canada). The probe sensor used for these measurements was 6 cm in length and 1.3 mm in diameter. In order to study the temperature effect on the thermal conductivity of the nanofluids a thermostat bath was used.

The convective heat transfer mechanism was studied using an home-made setup. A schematic and photograph of the setup is shown in Fig. 1. It consists of a flow loop, a heat unit, a cooling part, and a measuring and control unit. The flow loop includes a pump with a flow control valve system, a reservoir, a collection tank and a test section. A straight stainless steel tube with 108 cm

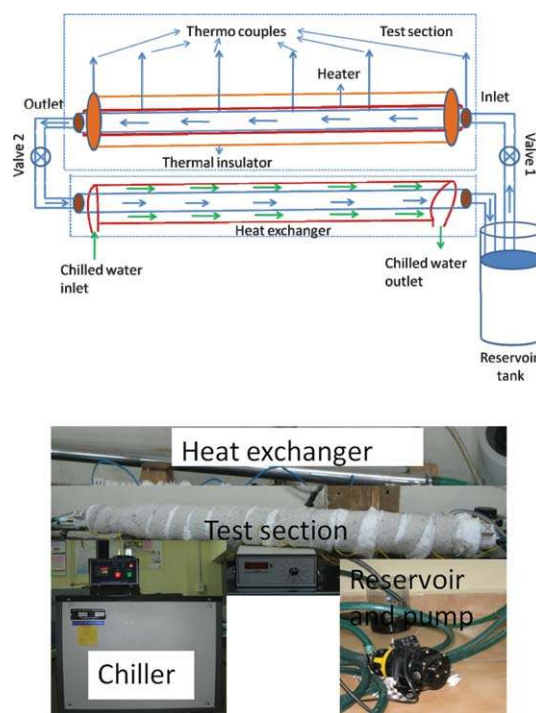


Fig. 1 Schematic (top) and photograph (bottom) of the fabricated heat transfer set up.

in length was used as the test section. The whole test section was heated by a copper coil linked to an adjustable DC power supply. There was a thick thermal isolating layer surrounding the heater to obtain a constant heat flux condition along the test section. Four T-type thermocouples were mounted on the test section at axial positions in mm of 298 (T1), 521 (T2), 748 (T3) and 858 (T4) from the inlet of the test section to measure the wall temperature distribution. Further, two T-type thermocouples were inserted into the flow at the inlet and exit of the test section to measure the bulk temperatures of nanofluids.

3. Results and discussion

3.1. XRD and Raman analysis

The crystallinity of the samples was studied using X-ray diffraction. Fig. 2A shows the XRD of f-MWNT, f-HEG and f-MWNT+f-HEG. The f-MWNT show a sharp but wide peak at $\sim 26.7^\circ$, corresponding to the (002) plane of carbon.¹ For f-HEG there is a very broad peak ranging from $\sim 18^\circ$ to $\sim 30^\circ$ which indicates the amorphous nature of graphene.¹¹ But in the case of f-MWNT+f-HEG, the peak broadens initially like f-HEG and then forms a wide but sharp peak, like f-MWNT. The XRD of f-MWNT+f-HEG shown in Fig. 2A is similar to that reported by Fan *et al.*¹⁵ The crystal structure of the hybrid nanostructure is a mixture of f-MWNT and f-HEG.

Fig. 2B shows the Raman spectrum of f-MWNT, f-HEG and f-MWNT+f-HEG. The peaks around 1340 cm^{-1} and 1560 cm^{-1} are due to the D-band and G-band respectively. The sp^2 vibration of the carbon atoms in the material results in the characteristic G-band, as exhibited by most carbon based materials.^{11,31}

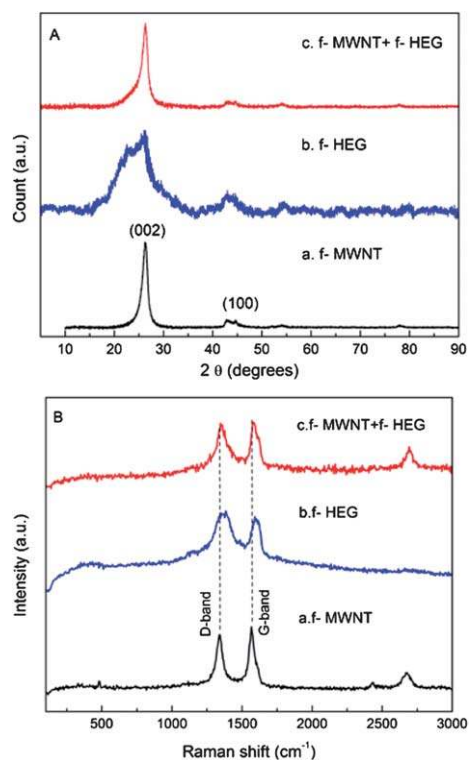


Fig. 2 (A) The X-ray diffractogram and (B) Raman spectra of f-MWNT, f-HEG and f-MWNT+f-HEG, respectively.

The D-band can be due to defects, disorder and impurities present in the material. This peak mainly suggests sp^3 hybridization of carbon atoms. In the case of functionalized carbon materials, the intensity of the D-band increases compared to that in the unfunctionalized material. During functionalization, an epoxy or a hydroxyl group is transformed from a planar sp^2 -hybridized state to a distorted sp^3 -hybridized geometry.⁸ This leads to an increase in the intensity of the D-band for f-HEG due to the disorder induced in the graphene sheet in the form of functional groups, folding, edges *etc.* In the case of f-MWNT, there is a small shoulder peak near the G-band at $\sim 1603\text{ cm}^{-1}$. The G- and D-bands are broad in the case of f-HEG. A universal observation is that higher disorder in graphite leads to a broader G-band, as well as to a broad D-band of a higher relative intensity compared to that of G-band.³² In the case of f-MWNT+f-HEG, the shoulder peak of f-MWNT merges with the broad peak of f-HEG. Table 1 shows the G- and D-band positions and the I_D/I_G ratio of f-MWNT, f-HEG and f-MWNT+f-HEG after Lorentzian fitting. I_D is the intensity of D-band and I_G is the intensity of G-band. The G-band and D-band positions of f-MWNT+f-HEG are intermediate between those of f-MWNT and f-HEG. The I_D/I_G ratio of f-MWNT and f-HEG is higher than that in unfunctionalized MWNT and HEG. This indicates an increase in the number of smaller MWNT and graphene domains. The I_D/I_G ratio of f-MWNT+f-HEG also lies between f-MWNT and f-HEG. This further confirms that f-MWNT+f-HEG is a hybrid of f-MWNT and f-HEG. (More details of the Raman data analysis are given in the ESI†).

3.2. Electron microscopy study

The surface morphology and structural studies of the MWNT, HEG and f-MWNT+f-HEG were carried out by FESEM and TEM, respectively. The corresponding images are shown in Fig. 3A–F. From the FESEM image of the MWNT shown in Fig. 3A, it is clear that there are no other impurities on the surface of the purified MWNT. The FESEM image of HEG (Fig. 3B) shows a wrinkled morphology, which is expected for any exfoliated graphene. The surface morphology of f-MWNT+f-HEG is shown in Fig. 3C. f-MWNT and f-HEG are homogeneously mixed in the hybrid nanostructure. Fig. 3D shows a TEM image of the MWNT. The outer diameter of the MWNT is around 30–40 nm. Fig. 3E clearly shows the wrinkled morphology and folding at the planar and edge portions of the graphene sheets. The TEM image (Fig. 3F) of f-MWNT+f-HEG shows the mixture of f-MWNT and f-HEG.

3.3. Thermal conductivity of the nanohybrid

The thermal conductivity of different volume fractions of the nanofluids were measured at different temperatures. Fig. 4A

Table 1 Position of G- and D-band along with their intensity ratios for f-MWNT, f-HEG and f-MWNT+f-HEG

Sample	G-band position	D-band position	I_D/I_G
f-MWNT	1568 cm^{-1}	1339 cm^{-1}	0.9907
f-HEG	1599 cm^{-1}	1366 cm^{-1}	1.008
f-MWNT+f-HEG	1589 cm^{-1}	1357 cm^{-1}	0.9927

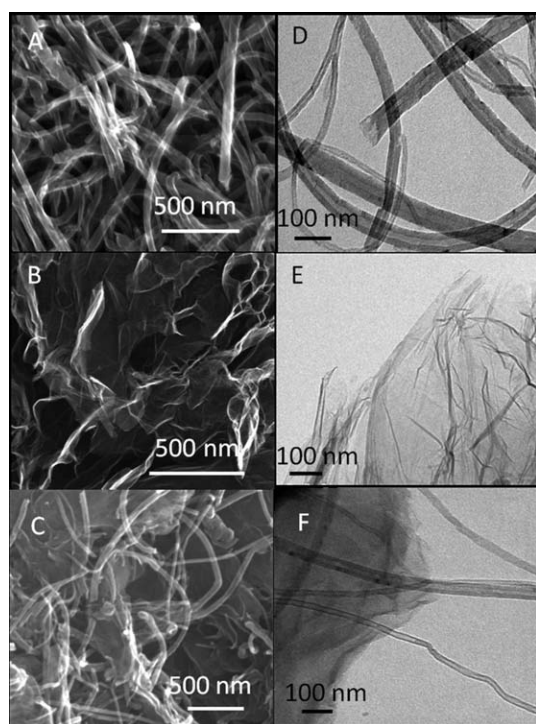


Fig. 3 FESEM (A–C) and TEM (D–F) images of MWNT, HEG and f-MWNT+f-HEG, respectively.

shows the thermal conductivity of the hybrid nanostructure in DI water. Error bars are also shown along with the data points. The thermal conductivity of DI water increases with increasing volume fraction. The percentage enhancement in thermal conductivity was calculated using the relation $((k - k_0) \times 100) / k_0$, where ' k_0 ' is the thermal conductivity of base fluid and ' k ' is that of nanofluid. The enhancement in thermal conductivity for volume fractions 0.005% and 0.05% is $\sim 9\%$ and $\sim 20\%$, respectively. The thermal conductivity of the nanofluid increases with increasing temperature also. For a 0.005% volume fraction at 30 °C the enhancement is $\sim 9\%$ and at 50 °C the enhancement is $\sim 12\%$. For a 0.05% volume fraction the enhancement is $\sim 20\%$ at 30 °C and $\sim 80\%$ at 50 °C. A similar trend is observed for all the volume fractions. The enhancement in thermal conductivity is better than that reported by Beck *et al.*³³ for a 5% volume fraction of CNT in water and by Xie *et al.*³⁴ for Al_2O_3 . Fig. 4B shows the thermal conductivity of the f-MWNT+f-HEG dispersed EG based nanofluid for different volume fractions at different temperatures. The EG based nanofluids did not show much enhancement in thermal conductivity for low volume fractions. For a 0.05% volume fraction the EG based nanofluid showed an enhancement of hardly 1% at 30 °C and $\sim 3\%$ at 50 °C. An enhancement of $\sim 2\%$ is observed for a volume fraction of 0.08% at 30 °C and an enhancement of $\sim 6\%$ at 50 °C. To minimize error in the measurement eight readings were taken at each temperature for a particular volume fraction, and the average of these values was taken as the thermal conductivity at that temperature.

The trend in enhancement suggests that thermal conductivity can be further increased by increasing the volume fraction. To test this assertion, we carried out thermal conductivity measurements for higher volume fractions (0.1% and 0.2%) of

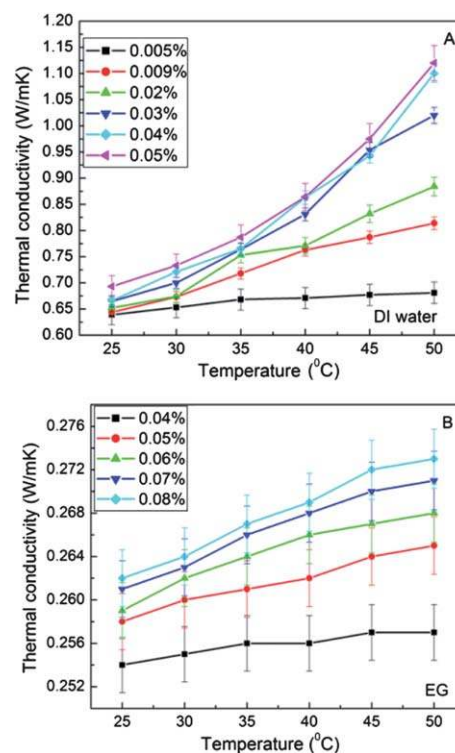


Fig. 4 Thermal conductivity of f-MWNT+f-HEG dispersed in (A) DI water and (B) EG based nanofluids for different volume fractions at different temperatures.

f-MWNT+f-HEG, at room temperature. Surprisingly, the enhancement in thermal conductivity was comparable to that of the 0.05% volume fraction, even though we could completely disperse the hybrid nanostructure both in DI water and EG. Further work in this direction is being carried out.

3.4. Convective heat transfer

The heat transfer coefficient (h) is a macroscopic parameter describing heat transfer when a fluid flows across a solid surface maintained at different temperature, and is not a material property. The convective heat transfer coefficient is defined as

$$h = q / (T_s(x) - T_f(x)) \quad (1)$$

where x represents axial distance from the entrance of the test section, q is the heat flux, T_s is the measured wall temperature, and T_f is the fluid temperature decided by the following energy balance:

$$T_f = T_{in} + E(x) / (M c_p) \quad (2)$$

where c_p is the heat capacity, M is the mass flow rate and $E(x)$ is the energy at position x . Eqn (2) is based on an assumption of zero heat loss through the insulation layer.

$$E(x) = (\text{Total energy} \times x) / \text{length of the tube} \quad (3)$$

Mass flow rate can be calculated using the relation,

$$M = uA\rho \quad (4)$$

where u is the velocity of flow, A is the area of cross section and ρ is the density of fluid. Reynolds number (Re) is defined as $Re = \rho u D / \mu$ and the Prandtl number is defined as $Pr = \nu / \alpha$, where μ is the fluid dynamic viscosity, ν is the fluid kinematic viscosity and α is the fluid thermal diffusivity.

3.4.1. Validity of the experimental setup with DI water. To check the reliability and accuracy of home-made experimental setup, systematic measurements were carried out using DI water. The validity of the experimental setup was tested for both laminar and turbulent flow. The experimental results obtained for laminar and turbulent flow were correlated with the well known Shah correlation³⁵ and Dittus–Boelter³⁶ equation, respectively, under the constant heat flux boundary condition. The Shah correlation is given as

$$Nu = \begin{cases} 1.953 \left(Re Pr \frac{D}{X} \right)^{1/3} & \left(Re Pr \frac{D}{X} \right) \geq 33.3 \\ 4.364 + 0.0722 Re Pr \frac{D}{X} & \left(Re Pr \frac{D}{X} \right) < 33.3 \end{cases} \quad (5)$$

where Nu is the Nusselts number. The experimental values are in reasonably good agreement with the Shah equation, as shown in Fig. 5a. The same is also observed for other laminar flow rates. For a high Reynolds number, the Dittus–Boelter equation is given below:

$$Nu = 0.023 Re^{0.8} Pr^{0.4} \quad (6)$$

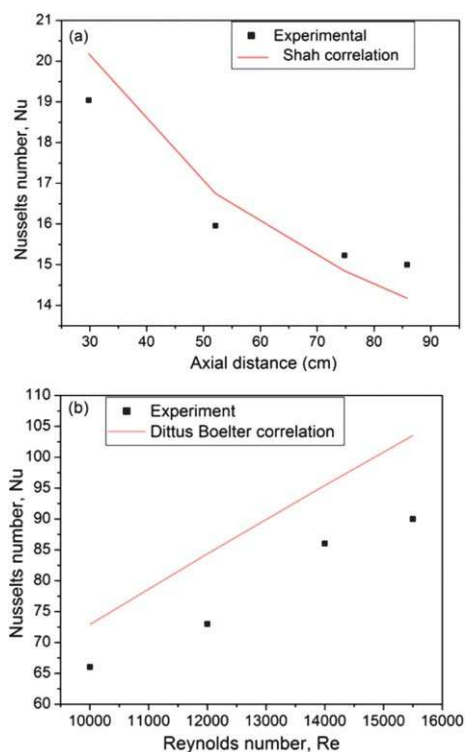


Fig. 5 Validity of the experimental heat transfer setup for (a) low flow rate and (b) high flow rate using water.

As shown in Fig. 5b, the good agreement between the experimental results and the calculated values for water reveals that the precision of the experimental system is good. The uncertainty of the experimental system is less than 8%.

3.4.2. Convective heat transfer of f-MWNT+f-HEG. Heat transfer experiments were conducted for different volume fractions of f-MWNT+f-HEG dispersed water based nanofluids for different flow rates (Reynolds numbers). For water based nanofluids the Reynolds numbers used were 4500, 8700 and 15 500, which model turbulent flow. The experiments were conducted for a constant input heat flux. The volume fractions chosen for the study were 0.005% and 0.01%. Fig. 6 shows a graph of the calculated heat transfer coefficient *versus* the axial distance for different Reynolds numbers for 0.005% (green solid line) and 0.01% (red dashed line) volume fractions. The results of the heat transfer of DI water (blue dotted lines) is also shown, for comparison purposes. The triangle represents $Re = 4500$, circle represents $Re = 8700$ and star represents $Re = 15 500$. The error in the measurement is less than 5%. For all the samples studied, the graph suggests that the heat transfer coefficient increases with increasing Reynolds number. Another observation is that the heat transfer coefficient decreases with increasing axial distance *i.e.* it decreases when going away from the starting point of the heat section. Theoretically, at the entrance of the heat section the boundary line thickness is zero. So, the heat transfer coefficient should be infinity here. The boundary layer increases with axial distance until fully developed, after which the boundary layer thickness and hence the convective heat transfer coefficient is constant.

At a constant Reynolds number, the heat transfer coefficient increases with an increasing volume fraction of f-MWNT+f-HEG. Out of the three curves, the 0.01% volume fraction shows the highest heat transfer coefficient. The trend is same for the circle (\circ) and star (\star) values too. For DI water based nanofluids (Fig. 6), it is evident that the heat transfer coefficients are high compared to that of the base fluid. The heat transfer coefficient increases with increasing volume fraction. The percentage enhancement in heat transfer was calculated using the relation

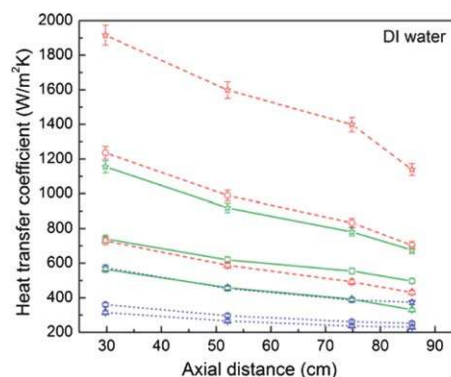


Fig. 6 Heat transfer measurement of f-MWNT+f-HEG dispersed water based nanofluid for volume fractions of 0.005% and 0.01%. The blue dotted lines, green solid lines and red dashed lines are for water alone, and the 0.005% and 0.01% volume fractions, respectively. $Re = 4500$ (Δ), $Re = 8700$ (\circ) and $Re = 15 500$ (\star).

$[h(x) - h_n(x)] \times 100/h(x)$, where $h(x)$ and $h_n(x)$ are the heat transfer coefficients for the base fluid and nanofluid at distance x . At the heat test section entrance for $Re = 4500$, the enhancement in the heat transfer coefficient is $\sim 181\%$ and $\sim 264\%$ for 0.005% and 0.01%, respectively. At the end of the heat test section, the enhancement is $\sim 166\%$ and $\sim 206\%$ respectively for volume fractions 0.005% and 0.01%. For $Re = 15\ 500$, the enhancement at the entrance is $\sim 259\%$ for 0.005% and $\sim 294\%$ for 0.01% volume fractions. At the exit, the enhancement is $\sim 178\%$ and $\sim 289\%$ respectively for 0.005% and 0.01% volume fractions.

Similar studies have also been carried out for EG based nanofluids. Fig. 7 shows the graph corresponding to volume fractions 0.005% and 0.01% for different Reynolds numbers ($Re = 250, 550, 1000$). The flow is laminar in nature. Here too blue dotted lines, green solid lines and red dashed lines represent EG alone, 0.005% volume fraction and 0.01% volume fraction respectively. Triangle (Δ), circle (\circ) and star (\star) correspond to $Re = 250, 550$ and 1000 , respectively. The trend in results is similar to what has been observed in the case of DI water based nanofluids. The heat transfer coefficient increases with volume fraction as well as the Reynolds number. At the heat test section entrance for $Re = 250$, the enhancement in the heat transfer coefficient is $\sim 273\%$ and $\sim 392\%$ for 0.005% and 0.01%, respectively. At the exit of heat section the enhancement is $\sim 207\%$ and $\sim 239\%$ respectively for volume fractions 0.005% and 0.01%. For $Re = 1000$, the enhancement at the entrance is $\sim 616\%$ for 0.005% and $\sim 697\%$ for 0.01% volume fractions. At the end portion the enhancements is $\sim 467\%$ and $\sim 672\%$ respectively for 0.005% and 0.01% volume fractions. Even though the enhancement in thermal conductivity is low for EG based nanofluids, the heat transfer coefficient is very high. The thermal conductivity and heat transfer coefficient of the f-MWNT+f-HEG hybrid nanostructure dispersed nanofluids are higher than that of the f-MWNT and f-HEG dispersed nanofluids.^{23,37}

The high thermal conductivity and heat transfer coefficient of f-MWNT+f-HEG dispersed DI water and EG based nanofluids can be attributed to the high aspect ratio of f-MWNT and f-HEG. In powder form, MWNT act like spacers between graphene layers which prevents the restacking of graphene, but in solution MWNT may act as good connectors between the

graphene sheets. (A pictorial representation is given in the ESI†) Moreover, as mentioned already, the hybrid nanostructure has a high surface area which helps more particles to come in contact with the liquid. When the volume fraction increases, the particle–particle contact also increases which aids in the continuous flow of heat. The enhancement in heat transfer is not only due to the enhancement in steady state thermal conductivity, but also due to the high surface area of nanomaterials, particle rearrangements and variation in the thermal boundary. It is anticipated that results will be more or less the same whichever synthesis procedure is adopted for making the graphene and MWNT hybrid nanostructure. More experiments are needed for a better understanding of the heat transfer mechanism.

4. Conclusion

A hybrid nanostructure (f-MWNT+f-HEG) has been synthesized and characterized by different experimental techniques. This hybrid nanostructure has been successfully dispersed in DI water and EG without any surfactant due to the proper functionalization of the hybrid nanostructure. The thermal transport properties for different volume fractions of the nanofluids have been systematically studied. The thermal conductivity and heat transfer coefficient increases with an increasing volume fraction of the hybrid nanostructure. At a particular concentration of hybrid nanostructure, the thermal conductivity increases with increasing temperature. Similarly, the heat transfer coefficient increases with an increase in Reynolds number. The high thermal conductivity and heat transfer coefficient values of f-MWNT+f-HEG dispersed nanofluids suggest that the nanofluids are potential candidates for coolant applications.

Acknowledgements

The authors would like to thank the Indian Institute of Technology Madras (IITM) and the Defence Research & Development Organisation (DRDO), India, for financial support.

Notes and references

- 1 A. Kaniyoor, R. I. Jafri, T. Arockiadoss and S. Ramaprabhu, *Nanoscale*, 2009, **1**, 382–386.
- 2 T. T. Baby and S. Ramaprabhu, *Talanta*, 2010, **80**, 2016–2022.
- 3 X. Wang, L. Zhi, N. Tsao, Z. Tomovic, J. Li and K. Muellen, *Angew. Chem., Int. Ed.*, 2008, **47**, 2990–2992.
- 4 S. A. Chesnokov, V. A. Nalimova, A. G. Rinzler, R. E. Smalley and J. E. Fischer, *Phys. Rev. Lett.*, 1999, **82**, 343–346.
- 5 D. Wang, D. Choi, J. Li, Z. Yang, Z. Nie, R. Kou, D. Hu, C. Wang, L. V. Saraf, J. Zhang, I. A. Aksay and J. Liu, *ACS Nano*, 2009, **3**, 907–914.
- 6 K. S. Novoselov, A. K. Geim, S. V. Morozov, D. Jiang, Y. Zhang, S. V. Dubonos, I. V. Grigorieva and A. A. Firsov, *Science*, 2004, **306**, 666–669.
- 7 L. Wei, T. D. Ming, H. Y. Bing, Y. C. Hui, S. Z. Qiang, C. X. Cheng, C. C. Meng, H. P. Xiang, L. Chang and Y. Q. Hong, *ACS Nano*, 2009, **3**, 3730–3736.
- 8 H. C. Schniepp, J.-L. Li, M. J. McAllister, H. Sai, M. Herrera-Alonso, D. H. Adamson, R. K. Prud'homme, R. Car, D. A. Saville and I. A. Aksay, *J. Phys. Chem. B*, 2006, **110**, 8535–8539.
- 9 V. C. Tung, M. J. Allen, Y. Yang and R. B. Kaner, *Nat. Nanotechnol.*, 2009, **4**, 25–29.
- 10 P. R. Somani, S. P. Somani and M. Umeno, *Chem. Phys. Lett.*, 2006, **430**, 56–59.
- 11 A. Kaniyoor, T. T. Baby and S. Ramaprabhu, *J. Mater. Chem.*, 2010, **20**, 8467–8469.

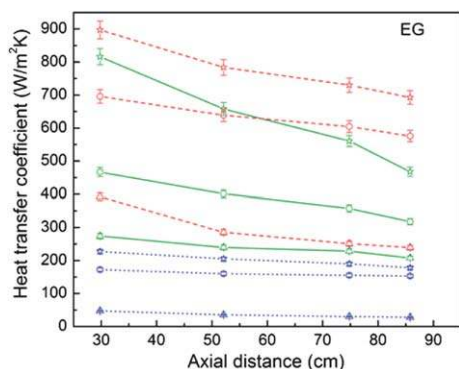


Fig. 7 Heat transfer measurement of f-MWNT+f-HEG dispersed ethylene glycol based nanofluid for volume fractions of 0.005% and 0.01%. Blue dotted lines, green solid lines and red dashed lines are for EG alone, and the 0.005% and 0.01% volume fractions, respectively. $Re = 250$ (Δ), $Re = 550$ (\circ) and $Re = 1000$ (\star).

- 12 S. J. Lee, H. K. Baik, J. Yoo and H. H. Jong, *Diamond Relat. Mater.*, 2002, **11**, 914–9717.
- 13 T. Guo, P. Nikolaev, A. Thess, D. T. Colbert and R. E. Smalley, *Chem. Phys. Lett.*, 1995, **243**, 49–54.
- 14 M. Yudasaka, R. Kikuchi, T. Matsui, Y. Ohki, S. Yoshimura and E. Ota, *Appl. Phys. Lett.*, 1995, **67**, 2477–2479.
- 15 Z. Fan, J. Yan, L. Zhi, Q. Zhang, T. Wei, J. Feng, M. Zhang, W. Qian and F. Wei, *Adv. Mater.*, 2010, **22**, 3723–3728.
- 16 V. C. Tung, L. M. Chen, M. J. Allen, J. K. Wassei, K. Nelson, R. B. Kaner and Y. Yang, *Nano Lett.*, 2009, **9**, 1949–1955.
- 17 E. J. Yoo, J. Kim, E. Hosono, H. Zhou, T. Kudo and I. Honma, *Nano Lett.*, 2008, **8**, 2277–2282.
- 18 S. U. S. Choi, Z. G. Zhang, W. Yu, F. Lockwood and E. A. Grulke, *Appl. Phys. Lett.*, 2001, **79**, 2252–2254.
- 19 J. A. Eastman, S. U. S. Choi, S. Li, W. Yu and L. Thompson, *Appl. Phys. Lett.*, 2001, **78**, 718–720.
- 20 S. Berber, Y. Kwon and T. Domanek, *Phys. Rev. Lett.*, 2000, **84**, 4613–4616.
- 21 P. Kim, L. Shi, A. Majumdar and P. L. McEuen, *Phys. Rev. Lett.*, 2001, **87**, 215502–4.
- 22 K. Saito, J. Nakamura and A. Natori, *Phys. Rev. B: Condens. Matter Mater. Phys.*, 2007, **76**, 115409–4.
- 23 N. Jha and S. Ramaprabhu, *J. Phys. Chem. C*, 2008, **112**, 9315–9319.
- 24 M.-S. Liu, M. C.-C. Lin, I.-T. Huang and C.-C. Wang, *Int. Commun. Heat Mass Transfer*, 2005, **32**, 1202–1210.
- 25 W. Yu, H. Xie and D. Bao, *J. Appl. Phys.*, 2010, **107**, 094317–6.
- 26 T. T. Baby and S. Ramaprabhu, *J. Appl. Phys.*, 2010, **108**, 124308–6.
- 27 Y. Ding, H. Alias, D. Wen and R. A. Williams, *Int. J. Heat Mass Transfer*, 2006, **49**, 240–250.
- 28 S. D. Park, S. W. Lee, S. Kang, I. C. Bang, J. H. Kim, H. S. Shin, D. W. Lee and D. W. Lee, *Appl. Phys. Lett.*, 2010, **97**, 023103–3.
- 29 M. M. Shaijumon and S. Ramaprabhu, *Chem. Phys. Lett.*, 2003, **374**, 513–520.
- 30 W. S. Hummers and R. E. Offeman, *J. Am. Chem. Soc.*, 1958, **80**, 1339.
- 31 H.-L. Wu, Y.-T. Yang, C.-C. Ma and H.-C. Kuan, *J. Polym. Sci., Part A: Polym. Chem.*, 2005, **43**, 6084–6093.
- 32 K. N. Kudin, B. Ozbas, H. C. Schniepp, R. K. Prud'homme, I. A. Aksay and R. Car, *Nano Lett.*, 2008, **8**, 36–41.
- 33 M. P. Beck, Y. Yuan, P. Warriar and A. S. Teja, *J. Nanopart. Res.*, 2010, **12**, 1469–1477.
- 34 H. Xie, J. Wang, T. Xi, Y. Liu, F. Ai and Q. Wu, *J. Appl. Phys.*, 2002, **91**, 4568–5.
- 35 R. K. Shah, Thermal entry length solutions for the circular tube and parallel plates, in *Proc. 3rd National Heat Mass Transfer Conference*. Indian Institute of Technology, Bombay, 1975, 1, Paper no. HMT-11-75.
- 36 F. W. Dittus and L. M. K. Boelter, Heat Transfer in Automobile Radiators of the Tubular Type, *Uni. of California Pub. in Eng.*, 1930, **2**, 443–461.
- 37 T. T. Baby and S. Ramaprabhu, *Nanoscale Res. Lett.*, accepted.